Title

APTO-253 stabilizes G-quadruplex DNA, inhibits MYC expression and induces DNA damage in acute myeloid leukemia cells

Journal

Molecular Cancer Therapeutics, 17(6)

ISSN

1535-7163

Authors

Local, Andrea
Zhang, Hongying
Benbatoul, Khalid D
et al.

Publication Date

2018-06-01

DOI

10.1158/1535-7163.mct-17-1209

Peer reviewed

Published OnlineFirst April 6, 2018; DOI: 10.1158/1535-7163.MCT-17-1209

Small Molecule Therapeutics

Molecular Cancer Therapeutics

APTO-253 Stabilizes G-quadruplex DNA, Inhibits MYC Expression, and Induces DNA Damage in Acute Myeloid Leukemia Cells

Andrea Local[1], Hongying Zhang[1], Khalid D. Benbatoul[1], Peter Folger[1], Xia Sheng[1], Cheng-Yu Tsai[2], Stephen B. Howell[2], and William G. Rice[1]

Abstract

APTO-253 is a phase I clinical stage small molecule that selectively induces CDKN1A (p21), promotes G_0–G_1 cell-cycle arrest, and triggers apoptosis in acute myeloid leukemia (AML) cells without producing myelosuppression in various animal species and humans. Differential gene expression analysis identified a pharmacodynamic effect on MYC expression, as well as induction of DNA repair and stress response pathways. APTO-253 was found to elicit a concentration- and time-dependent reduction in MYC mRNA expression and protein levels. Gene ontogeny and structural informatic analyses suggested a mechanism involving G-quadruplex (G4) stabilization. Intracellular pharmacokinetic studies in AML cells revealed that APTO-253 is converted intracellularly from a monomer to a ferrous complex [$Fe(253)_3$]. FRET assays demonstrated that both monomeric APTO-253 and $Fe(253)_3$ stabilize G4 structures from telomeres, MYC, and KIT promoters but do not bind to non-G4 double-stranded DNA. Although APTO-253 exerts a host of mechanistic sequelae, the effect of APTO-253 on MYC expression and its downstream target genes, on cell-cycle arrest, DNA damage, and stress responses can be explained by the action of $Fe(253)_3$ and APTO-253 on G-quadruplex DNA motifs. *Mol Cancer Ther; 17(6); 1177–86. ©2018 AACR.*

Introduction

APTO-253, a small-molecule 2-indolyl imidazole [4,5-d] phenanthroline derivative, is currently undergoing clinical development for the treatment of acute myeloid leukemia (AML). It has broad *in vitro* cytotoxicity in various human tumor cell lines, including solid tumors, leukemias, and lymphomas (1). APTO-253 has antitumor activity in murine xenograft models of the human solid tumors and was advanced into a phase I clinical trial in patients with advanced solid tumors (NCT123226; refs. 1–3). In that solid tumor clinical trial, APTO-253 was well tolerated and produced evidence of antitumor activity in patients with advanced refractory solid tumors but did not produce myelosuppression even at the maximum tested dose. The most common treatment-emergent adverse effects of any grade were rash, peripheral neuropathy, hypersensitivity (<10%), and fatigue (>10%; ref. 4). Recently, APTO-253 was tested for activity against primary cultures of leukemic mononuclear cells freshly isolated from 177 patients with hematologic malignancies through the BEAT AML Project (http://www.lls.org/beat-aml). Among the 80 AML patient samples tested, 43 (54%) were responsive to APTO-253 with an IC_{50} <1 μmol/L (5). Because of its antitumor activity against AML cells, and because of its safety profile observed in the solid tumor clinical trial, APTO-253 was advanced into a phase I clinical trial in patients with relapsed/refractory hematologic malignancies (NCT02267863) with emphasis on AML.

The purpose of the current investigation was to gain a more complete understanding of the molecular mechanism through which APTO-253 kills AML cells. We report here that APTO-253 is associated with CDKN1A upregulation and MYC downregulation, followed by G_0–G_1 cell-cycle arrest and apoptosis in AML cells. Moreover, inhibition of MYC, a well-recognized pivotal oncogene in AML, correlated with the cytotoxicity of APTO-253. Differential expression analysis suggested the involvement of DNA damage, including induction of γ-H2AX accumulation, and cellular stress pathways after APTO-253 treatment. Prior cellular pharmacokinetic studies demonstrated that APTO-253 is transformed from a monomeric form to a ferrous complex [$Fe(253)_3$] in cells, and that this complex is the principal intracellular form of the drug (6). In this study, we demonstrate that the parental APTO-253 and the $Fe(253)_3$ complex bind to and stabilize G-quadruplex (G4) motifs. The $Fe(253)_3$ complex stabilized G4 motifs found in the promoters of key oncogenes (e.g., *MYC, KIT*), as well as in rRNA genes and telomeres. This stabilization of secondary DNA structures was specific for G4 motifs, as the parental APTO-253 and $Fe(253)_3$ did not interact with ds-DNA. Treatment of MV4-11 AML cells with preformed $Fe(253)_3$ also inhibits MYC expression and induces CDKN1A expression along with induction of apoptotic and DNA damage pathways. Together, the results support the conclusion that the effect of APTO-253 on the expression of MYC and its downstream target genes, on cell-cycle arrest, and on DNA damage and stress responses can be linked to the action of APTO-253 and the $Fe(253)_3$ on G-quadruplex DNA motifs.

[1]Aptose Biosciences Inc., San Diego, California. [2]Moores Cancer Center and Department of Medicine, University of California, San Diego, California;

Note: Supplementary data for this article are available at Molecular Cancer Therapeutics Online (http://mct.aacrjournals.org/).

A. Local and H. Zhang contributed equally to this article.

Corresponding Author: William G. Rice, Aptose Biosciences Inc., 12770 High Bluff Drive, Suite 120, San Diego, CA 92130. Phone: 858-926-2747; E-mail: wrice@aptose.com

doi: 10.1158/1535-7163.MCT-17-1209

Published OnlineFirst April 6, 2018; DOI: 10.1158/1535-7163.MCT-17-1209

Materials and Methods

Cells and compounds

EOL-1, GRANTA-519, Jeko-1, Jurkat, Molm-13, NOMO-1, SKM-1, and SU-DHL-6 were obtained from Leibniz-Institut DSMZ. HL-60, KG-1, Mino, MV4-11, Raji, and THP-1 were obtained from ATCC. HEL92.1.7 were obtained from the European Collection of Authenticated Cell Cultures and Ramos cells were a gift from Dr. M. Andreeff (MD Anderson Cancer Center, Houston, TX). All cells were cultured in complete media as per the manufacturer's instructions. Early passage cells were collected and frozen within 1 month of receipt from the manufacturer. All experiments were performed on early passage cells within 6 weeks of thawing. MycoScope Mycoplasma Detection Kit (Genlantis catalog # MY01050) was used to screen for potential contamination every 6 months. Peripheral blood mononuclear cells (PBMC) were isolated from fresh healthy donor blood using Ficoll-Paque PLUS (GE Healthcare, catalog #17-1440-02). For synthesis of APTO-253 free base, 10-phenanthroline-5,6-dione (1.2 equivalents), acetic acid (22 volumes), 2-methyl-5-fluoroindole-3-carboxaldehyde (1.0 equivalents), and ammonium acetate (15 equivalents) were reacted under medium agitation while heated at 95 ± 5°C for 3 to 7 hours. The reaction was cooled to between 20°C and 25°C, filtered, rinsed with acetic acid and ethanol, and dried with N_2 purge, followed by a wash with 2:1 ethanol: water at 65°C for 4 hours, cooling to 20°C to 25°C, filtration, rinsing with 2:1 ethanol:water and EtOAc, and then dried with N_2 purge. The purity by HPLC was 99.5%, and the structural identity was confirmed by FT-IR, ^{1}HNMR, ^{13}C NMR, and LC/MS. For $Fe(253)_3$ synthesis, five molar equivalents of ferrous ion $FeS0_4$ in water was added to APTO-253 dissolved in ethanol. The deep red precipitate produced, $Fe(253)_3$, was collected and dissolved in DMSO and characterized by HPLC and mass spectrometry as >95% pure. CX-5461 (7) was purchased from MedChem Express (catalog # HY-13323).

Cytotoxicity study

Cells were plated and treated with vehicle DMSO or APTO-253 (10 concentrations) in 96-well plates for 5 days at 37°C and 5% CO_2. Cell viability was measured using CellTiter 96 AQ_{ueous} one solution (MTS) cell proliferation assay (Promega, catalog #G3581), and IC_{50} values were calculated using GraphPad Prism 7 software.

Uptake and efflux assay

Cells exposed to APTO-253 were homogenized in acetonitrile containing 5 ng of deuterated APTO-253 standard. Samples were analyzed at the UCSD Molecular Mass Spectrometry Facility employing an Agilent 1260 liquid chromatograph (LC) system coupled with a Thermo LCQdeca mass spectrometer using positive ion mode electrospray ionization as the ion source.

qRT-PCR

Cells were treated with vehicle or APTO-253 at various concentrations for 24 hours or at a single concentration for 1, 3, 6, 12, and 24 hours before harvesting. Cells were lysed by QiaShredder columns (QIAGEN, catalog # 79656), total RNA was isolated using QIAGEN RNeasy Plus Mini Kit (catalog # 74134), and cDNA was synthesized utilizing Transcriptor Universal cDNA master mix (Roche, catalog # 05893151001) and then used for qRT-PCR analysis using FastStart essential DNA probes master mix (Roche, catalog # 06402682001) and Roche LightCycler96. Primer probe pairs were purchased from IDT (Supplementary Table S1). Expression was calculated as fold change over vehicle treated samples after normalizing to *GAPDH* ($2^{\Delta\Delta C}{}_t$).

Western blotting

Cells were treated as described above. Whole-cell lysates were prepared, separated by SDS-PAGE, and transferred to nitrocellulose membranes. Detection antibodies used are listed in Supplementary Table S2. Densitometry was performed using ImageJ or Image Studio Lite Version5.2 software and normalized to the density of GAPDH.

Flow cytometry for apoptosis and cell-cycle analysis

Cells were treated as described above. To determine apoptosis, cells were stained with FITC-Annexin V and propidium iodide (PI; BD Pharmingen, catalog #556570) and then analyzed on BD Accuri C6 flow cytometer. To measure DNA synthesis and phases of cell cycle, treated cells were stained with 5-ethynyl-2′-deoxyuridine (Edu) Alexa Fluor 488 (Thermo Fisher Scientific, catalog #C10425) and PI (PI/RNase A staining solution, BD Biosciences, catalog #550825). The dead cells were excluded from analysis by using Live/Dead Fixable Far Red Dead Cell Stain Kit (Thermo Fisher Scientific, catalog # L34973). Staining was performed as per the manufacturers' instructions.

RNA sequencing analysis

Treated MV4-11 cells were subjected to total RNA extraction (as for qRT-PCR analysis) and sequenced at the UCSD genomics core facility. RNA was processed using Illumina TruSeq and single end sequenced for 50-bp reads on the Illumina HiSeq4000. Data were analyzed by the McWeeny lab at Oregon Health and Science University (Portland, OR). FASTQ files were assessed for read base distribution and sequence representation using FASTQC http://www.bioinformatics.babraham.ac.uk/projects/fastqc/. Reads were aligned to HG37 using SubRead v1.5.0-pl keeping uniquely mapped reads (8). Differential expression genes with less than 50 reads (across all 4 samples) were discarded. Raw data and processed files are available on GEO (https://www.ncbi.nlm.nih.gov/geo/query/acc.cgi?acc=GSE111949) accession number GSE111949.

Reverse-phase protein array analysis

MV4-11 cells were treated as for RNA sequencing (RNA-seq) analysis and whole-cell extracts were prepared for Western blotting. Samples were processed at MD Anderson Cancer Center reverse-phase protein array (RPPA) core facility (details at https://www.mdanderson.org/research/research-resources/core-facilities/functional-proteomics-rppa-core/rppa-process.html). Protein expression levels were averaged for 3 replicates and heatmaps were drawn using GraphPad Prism 7.

Chromatin immunoprecipitation coupled with qPCR

MV4-11 cells were treated with vehicle DMSO or 500 nmol/L APTO-253 for 2, 6, or 24 hours and then crosslinked with 1% formaldehyde. Chromatin was extracted by sonication and then incubated with H3K27ac (Active Motif #39133) antibody overnight. The antibody:DNA complexes were isolated with Protein G beads (Invitrogen Dynabeads catalog #10004D) and analyzed by qPCR with primers specific to the MYC promoter (Supplementary

Published OnlineFirst April 6, 2018; DOI: 10.1158/1535-7163.MCT-17-1209

Table S3). H3K27ac enrichment was calculated as fold over input DNA control.

RNA decay assay

Cells were treated for 3 hours with vehicle DMSO or 500 nmol/L APTO-253 followed by 1 μmol/L actinomycin D. Aliquots of cells were taken before and then every 10 minutes after actinomycin D addition for RNA extraction and cDNA synthesis as for qRT-PCR analysis. Levels of MYC and 28s rRNA were analyzed using specific primers (Supplementary Table S4) and MYC RNA expression was normalized to 28s rRNA [2^(28s C_t value – MYC C_t value)].

FRET assay

FRET assay and data analysis was performed as described previously (9, 10) and modified by using dual labeled (5′ FAM – 3′ BHQ1) single-stranded oligos. Melting temperature of each oligo was assessed in the presence of vehicle DMSO or escalating concentrations of APTO-253, $Fe(253)_3$, CX-5461, or TMPyP4 using a Roche LightCycler 96 [at 37°C for 300 seconds followed by temperature increased in 3°C intervals up to 91°C (25 steps) with 300-second total incubation time at each temperature]. Drug and oligo reaction mixes were analyzed immediately or incubated for 6 hours at room temperature and then analyzed. Primer information is provided in Supplementary Table S5. Longer incubation time did not affect $Fe(253)_3$, TMPyP4, or CX-5461 activity but enhanced APTO-253 G4–binding ability. APTO-253 data are presented for 6-hour time point.

Results

APTO-253 induces cytotoxicity, upregulates p21, and induces G_0–G_1 cell-cycle arrest in AML cells

APTO-253 inhibited proliferation in AML cell lines and various forms of lymphoma cell lines with IC_{50} values ranging from 57 nmol/L to 1.75 μmol/L (Fig. 1; Supplementary Table S6). The drug showed only modest variation in potency as a function of duration of exposure in MV4-11 cells with IC_{50} values of 0.47, 0.40, and 0.24 μmol/L for exposures of 48, 72, and 120 hours, respectively. Previous studies reported upregulation of KLF4 and CDKN1A expression as a potential mechanism of APTO-253 activity in tumors (2–5, 11, 12). Although APTO-253 upregulates KLF4 expression in 4 of 6 AML cell lines tested (Supplementary Fig. S1A), *CDKN1A* (*p21*) expression was induced in all AML cell lines in a concentration-dependent manner (Supplementary Fig. S1B and S1C). The upregulation of *CDKN1A* mRNA increased with duration of exposure in all AML cell lines tested (Supplementary Fig. S1D and S1E). At later time points, *CDKN1A* expression began to decrease, likely due to increasing cell death. Induction of CDKN1A expression is typically associated with a subsequent G_0–G_1 cell-cycle arrest, which was observed following APTO-253 treatment of solid tumor lines (1, 12, 13). Consistent with this, we observed a dose-dependent increase of cells in G_0–G_1 with concomitant reduction in the fraction of cells in the S- and G_2–M phases for all AML cell lines tested (Fig. 2A–C, top). In the case of MV4-11, all live cells had arrested in G_0–G_1 after 24-hour exposure to 1 μmol/L APTO-253. CCND3 (Cyclin D3) and CDK4 are known to promote G_1 cell-cycle progression, while CDKN1A serves to negatively regulate this process. Western blot analysis of APTO-253–treated AML cells revealed dose-dependent inhibition of both CDK4 and CCND3, albeit to different degrees in each of the 3 AML lines (Fig. 2A–C, bottom; Supplementary Fig. S2A).

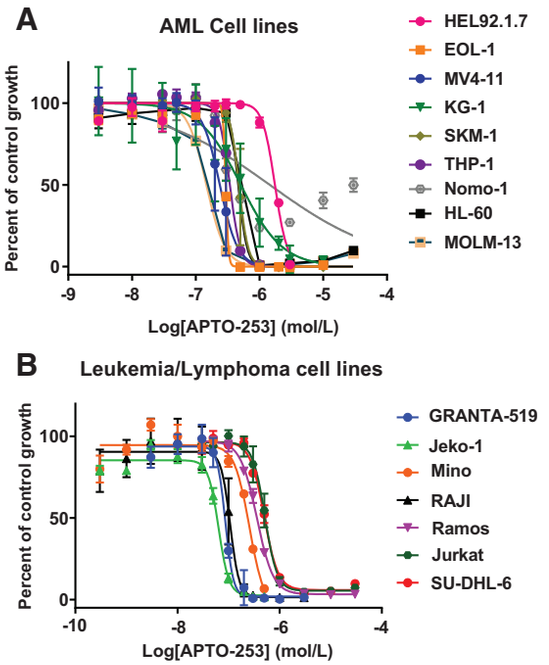

Figure 1.

Antiproliferative activity of APTO-253 against leukemia and lymphoma cell lines. **A,** Concentration-response curves for AML cell lines treated for 5 days with APTO-253. Cell growth expressed as percent of growth of vehicle-treated cells. **B,** Concentration-response curve for other leukemia and lymphoma cell lines. Error bars, ±SD of at least three replicate assays.

To correlate cell-cycle arrest with various pathway perturbations, and to delineate the sequence of mechanistic events, cell-cycle analyses were performed after treating cells with either vehicle or APTO-253 (IC_{50} concentration) for various times up to 24 hours. There was no perturbation of cell-cycle phase distribution in cells treated with vehicle alone. An increase in the fraction of cells in G_0–G_1 was detected as early as 2 hours, and this fraction continued to increase in a time-dependent manner throughout the 24-hour period of drug exposure (Fig. 2D–F). Western blot analysis showed a time-dependent decrease of CDK4 and CCND3 protein levels that paralleled the G_0–G_1 arrest (Supplementary Fig. S2B and S2C). These data establish that APTO-253 produces a time- and concentration-dependent G_0–G_1 arrest in AML cells and suggest that this is mediated by established p21 and cyclin-dependent kinase pathways.

APTO-253 induces apoptosis in AML cell lines

To investigate the mechanism by which APTO-253 causes cell death, MV4-11, EOL-1, and KG-1 AML cells were treated with or without APTO-253 and subjected to apoptotic marker detection by flow cytometry and Western blotting. Cells were stained with PI and Annexin V to distinguish between live (Annexin V and PI negative), early apoptotic (Annexin V positive and PI negative), late apoptotic (Annexin V and PI positive), and dead (Annexin V negative and PI positive) cells. A concentration-dependent increase in apoptotic cells was observed at 24 hours in all cell lines (Fig. 3A; Supplementary Fig. S3A). The IC_{50} values based on Annexin V and PI staining paralleled antiproliferative IC_{50} values.

Published OnlineFirst April 6, 2018; DOI: 10.1158/1535-7163.MCT-17-1209

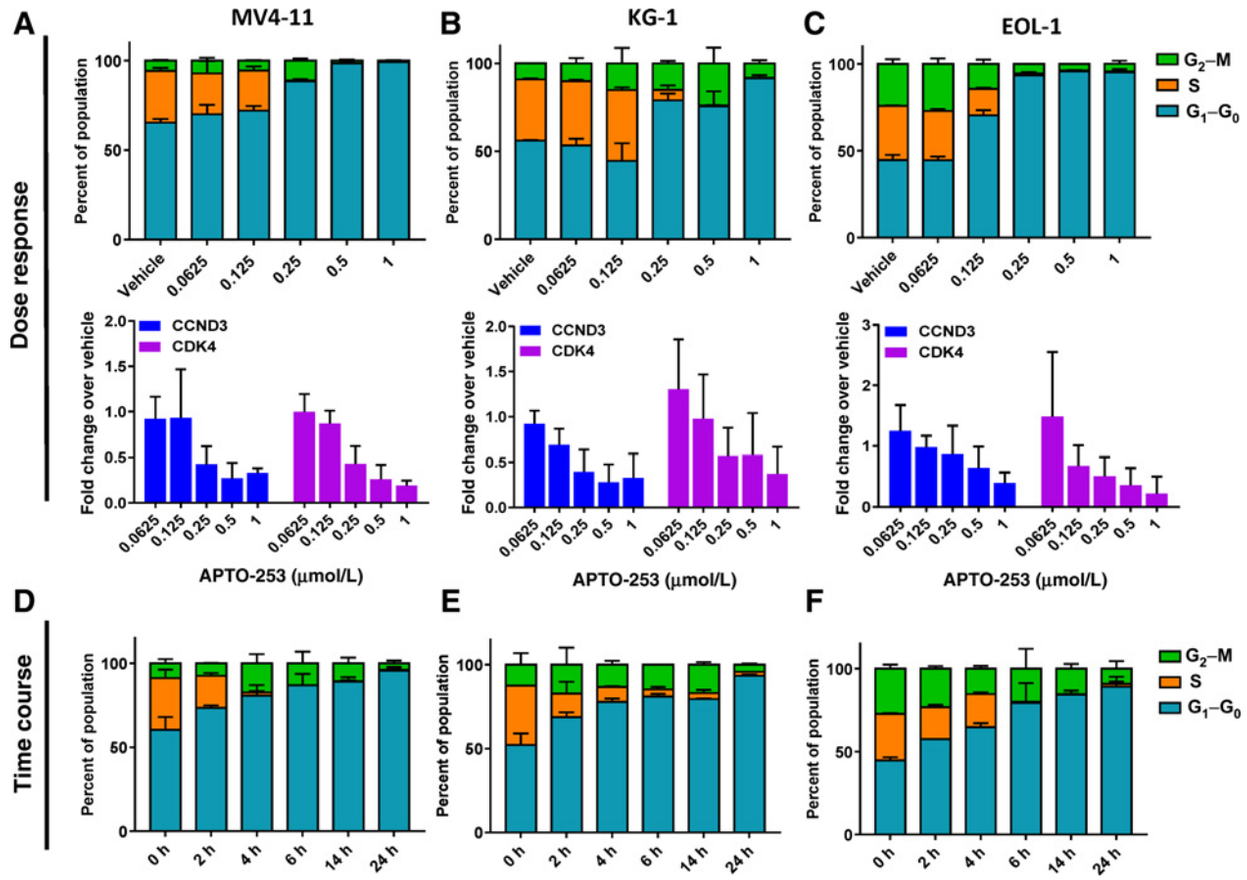

Figure 2.

APTO-253 induces G_0–G_1 cell-cycle arrest in a dose- and time-dependent manner in AML cell lines. **A,** Top, MV4-11 cells treated with APTO-253 at indicated concentrations for 24 hours. Cell-cycle distribution assayed as described in the Materials and Methods section. Bottom, CDK4 and CCND3 protein levels in MV4-11 cells after 24-hour exposure to APTO-253. Protein levels quantitated from three independent Western blots, graphed as fold change over vehicle. **B** and **C,** Effect of APTO-253 on cell-cycle distribution in KG-1 and EOL-1 cells. **D–F,** Effect of APTO-253 on cell-cycle distribution as a function of duration of exposure (MV4-11 cells, 500 nmol/L; KG-1 cells, 600 nmol/L APTO-253; and EOL-1 cells, 300 nmol/L APTO-253). Error bars, ± SD of two replicate assays for flow cytometry and three replicates for Western blots.

PARP cleavage (c-PARP1) is a classic signal of apoptosis downstream of both the intrinsic and extrinsic pathways. APTO-253 induced accumulation of c-PARP1 in a concentration- and time-dependent manner that paralleled apoptosis induction as measured by Annexin V/PI staining (Fig. 3B–C; Supplementary Fig. S3B). For all 3 AML cell lines, increases in apoptotic cells appeared between 3 and 6 hours after exposure to APTO-253 (Fig. 3D), which followed G_0–G_1 cell-cycle arrest observed at 2-hour exposure.

APTO-253 pharmacodynamics

To gain further insight into the pathways exploited by APTO-253 to cause cell-cycle arrest and apoptosis, we performed differential expression analysis at both the mRNA and protein levels. MV4-11 cells were treated with either vehicle or 500 nmol/L APTO-253 for 6 hours, and then gene expression was analyzed by RNA-seq. A total of 1,643 genes were found to be differentially regulated upon APTO-253 treatment (>2-fold change and $P < 0.05$) with 416 being upregulated and 1,227 being downregulated (Supplementary Table S7). The RNA-seq analysis detected a 2-fold increase in *KLF4* and a 4.5-fold increase in *CDKN1A* expression, which is validated by the qRT-PCR data with MV4-11 cells. The differentially regulated genes were analyzed for enriched pathways or GO (Gene Ontology) terms (Supplementary Fig. S4A) utilizing the Broad Molecular Signatures database (http://software.broadinstitute.org/gsea/msigdb/index.jsp). As expected, apoptotic and cell-cycle pathways were enriched in the differentially expressed gene set. Unexpectedly, gene expression profiles after APTO-253 treatment were also enriched in the DNA damage response (DDR) and endoplasmic reticulum (ER) stress/unfolded protein response pathways. In addition, upregulated genes were enriched in TP53 pathways and genes downregulated by MYC. Gene expression changes detected in MV4-11 cells raised the possibility that APTO-253 could cause apoptosis by inducing DNA damage and activating cellular stress pathways, and/or by inhibition of expression of the *MYC* oncogene.

To examine the effect of APTO-253 on protein expression, MV4-11 cells were treated as above and analyzed by RPPA microarray to quantify >300 total and posttranslationally modified proteins. Effects were observed on levels of both total and posttranslationally modified proteins (>1.25-fold and

Published OnlineFirst April 6, 2018; DOI: 10.1158/1535-7163.MCT-17-1209

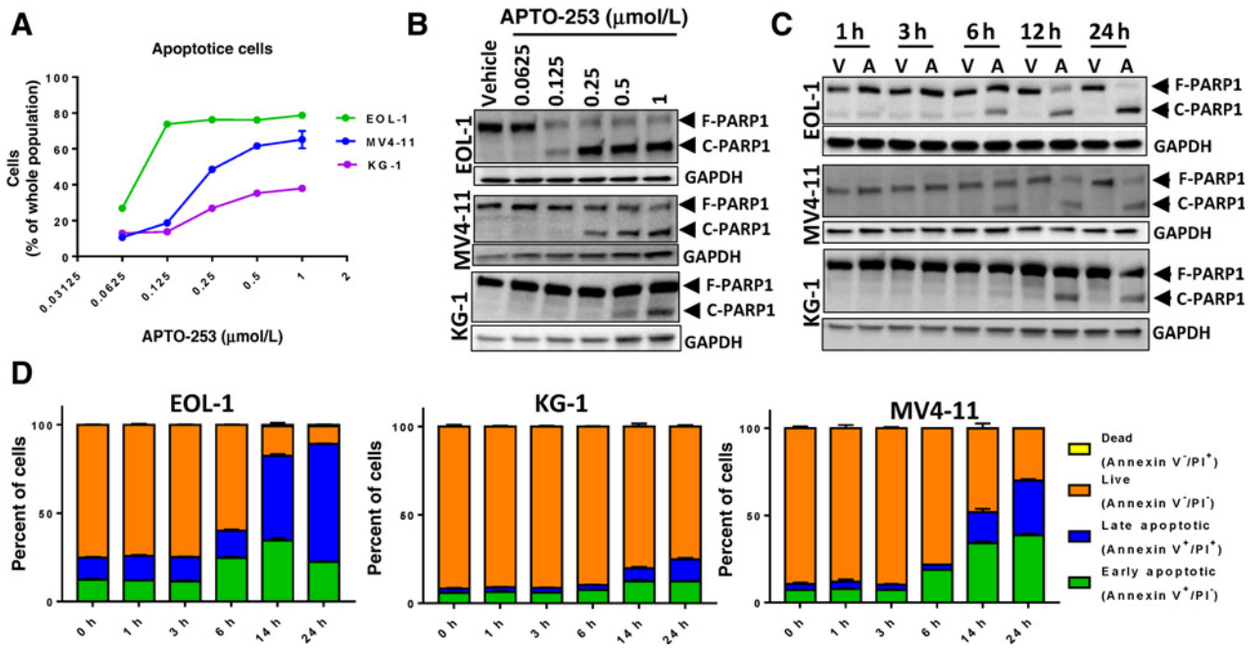

Figure 3.

APTO-253 treatment induces apoptosis in a time- and concentration-dependent manner. **A,** Percent apoptotic (early and late) MV4-11, KG-1, and EOL-1 cells after 24-hour exposure to APTO-253. Apoptosis was measured as described in the Materials and Methods section. **B,** Western blot analysis with PARP1-specific antibody of AML cells treated for 24 hours with V-vehicle or A-APTO-253. PARP1 antibody recognizes both full-length (upper band) and cleaved PARP1 (lower band). **C,** Western blot analysis of PARP1 cleavage in MV4-11, KG-1, and EOL-1 cells treated for 1 to 24 hours with 500 nmol/L of APTO-253. GAPDH is included as loading control. **D,** Time course of APTO-253 induced apoptosis in MV4-11 (500 nmol/L), KG-1 (600 nmol/L), and EOL-1 (300 nmol/L) cells. Error bars, ± SD of two replicate assays.

$P < 0.05$) with more proteins upregulated than downregulated (Supplementary Fig. S4B; Supplementary Table S7). Of note, there was an increase of cleaved caspase-7, which is indicative of apoptosis. GO analysis of the differentially expressed proteins was performed utilizing the Broad Molecular Signatures database. Significant GO terms included cell death and G_1–S cell-cycle arrest pathways, a formal description of G_0–G_1 arrest, and consistent with the cell-cycle effects detected by flow cytometry and the RNA-seq analyses (Supplementary Fig. S4C). An increase in E2F1, TP53, γH2AX, CHEK1 phos-S296, and CHEK2 phos-T68 supported the concept that DNA damage pathways are triggered by APTO-253 treatment (14). In addition, increases in XBP1, HSPA5, and MAPK14 (p38) phos-T180/182 were observed, indicating ER or cellular stress ($P = 1.89E^{-08}$; ref. 15). DDR pathways can also signal through the MAPK pathway activating MAPK14 and MAPK8 (JNK), and cross-talk between the DDR pathway and ER stress is a well-established phenomenon (14) although it is unclear which pathway represents the initiating event. A significant portion of the differentially expressed proteins and mRNAs are target genes of MYC oncoprotein, which is known to be an integral part of both cell-cycle and apoptotic pathway regulation. Collectively, these data suggested that regulation of the *MYC* oncogene may play an early and key role in the mechanism of APTO-253.

APTO-253 concentration- and time dependently downregulates MYC mRNA and protein levels in AML cells

MYC expression is implicated in the pathogenesis of a wide range of cancers, including leukemia and lymphoma (16). A recent study demonstrated that inhibition of *MYC* transcription leads to apoptosis in cancer cells of hematologic origin, making MYC an attractive therapeutic target (17, 18). A review of our RNA-seq dataset revealed that MYC was downregulated by APTO-253 in MV4-11 cells at 6 hours. We also observed increased transcription of genes negatively regulated by MYC in APTO-253–treated MV4-11 cells. APTO-253 produced a concentration-dependent decrease in both MYC mRNA and protein levels in all AML cell lines tested, and the IC_{50} values for MYC inhibition paralleled the antiproliferative IC_{50} values (Fig. 4A and B). These changes increased as a function of exposure time up to 24 hours in the MV4-11, EOL-1, and KG-1 AML cells (Fig. 4C; Supplementary Fig. S5A and S5B). The time course of MYC protein repression in MV4-11 cells paralleled inhibition of *MYC* gene expression levels detected by RNA-seq. All the tested AML cell lines had significantly higher basal expression of *MYC* as compared with PBMCs from healthy donors (Fig. 4D; Supplementary Fig. S5C). Thus, APTO-253 downregulates MYC at the mRNA and protein level in all AML cell lines examined.

Regulation of MYC expression is a complex process that involves *MYC* transcription, mRNA stability, and protein turnover (19). ChIP-qPCR analysis for H3K27ac, a well-established marker of active chromatin, was performed to assess transcriptional competency of the *MYC* gene promoter after treatment with APTO-253 (Supplementary Fig. S5D). A decrease in H3K27ac at the *MYC* promoter in MV4-11 cells was observed as early as 2 hours and progressed over time, indicating that modification of the *MYC* promoter and subsequent transcriptional repression of the *MYC* gene is an early mediator of the APTO-253 mechanism of action (Supplementary Fig. S5E). To determine whether

Published OnlineFirst April 6, 2018; DOI: 10.1158/1535-7163.MCT-17-1209

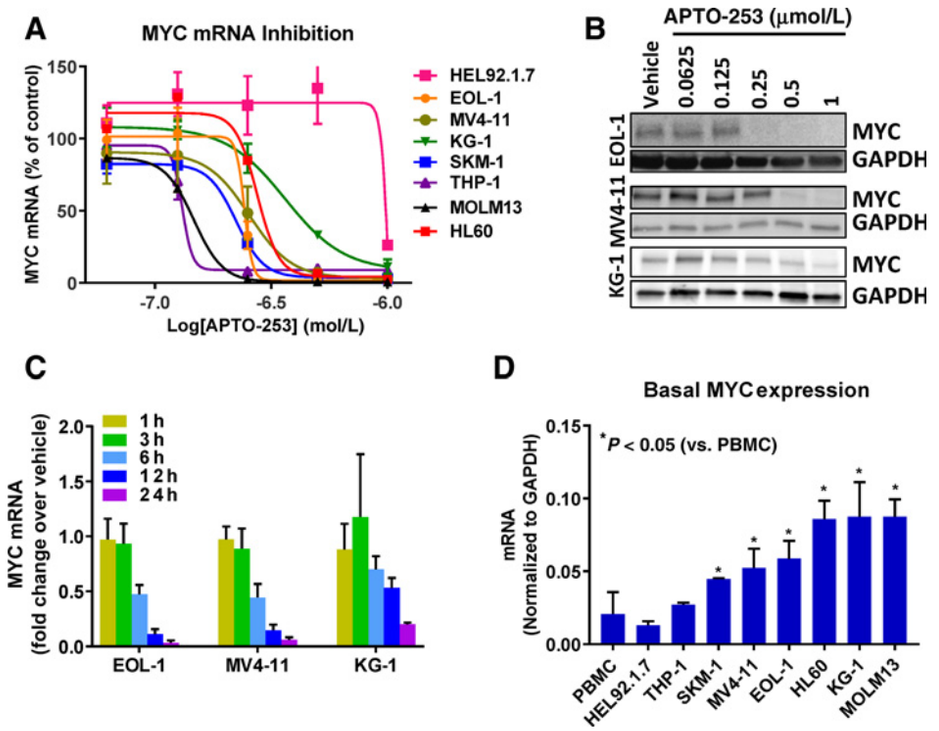

Figure 4.
MYC RNA and protein expression is negatively regulated by APTO-253. **A,** AML lines were treated for 24 hours and MYC mRNA levels measured by qRT-PCR with MYC-specific primer/probe pairs. Graphed as percent of vehicle using GraphPad Prism. **B,** Western blot analysis of MYC protein level in MV4-11, KG-1, and EOL-1 cells treated for 24 hours at the concentrations listed. GAPDH served as a loading control. **C,** Histogram plot of MYC mRNA expression graphed as fold change over vehicle in MV4-11, KG-1, and EOL-1 cells treated with 500 nmol/L APTO-253 for the times listed. **D,** Basal expression level of MYC mRNA in AML cell lines compared with PBMCs from healthy donors. Expression relative to GAPDH assayed by qRT-PCR. Error bars, ± SD from at least three replicate experiments.

APTO-253 affected MYC mRNA stability, an RNA decay assay was performed on EOL-1 cells. There was a clear decrease in MYC mRNA levels in the APTO-253 pretreated cells versus vehicle (Supplementary Fig. S5F), indicating that APTO-253 can decrease the stability of MYC mRNA. These data suggest that APTO-253 regulates MYC by affecting both transcription and mRNA stability.

APTO-253 triggers DNA damage and cellular stress pathways

In addition to MYC, RNA and protein differential expression analyses pointed to the involvement of TP53, DNA damage, and ER stress in the mechanism of action of APTO-253. We sought to validate the RPPA data that had demonstrated an increase in TP53 protein level after APTO-253 treatment in MV4-11 cells. Exposure of MV4-11 cells to 500 nmol/L APTO-253 produced a significant increase in TP53 levels at early time points (1, 3, and 6 hours), followed by a return to baseline at 12 hours and a further reduction at 24 hours, presumably due to extensive cell death at this time point (Fig. 5A). The increase in total protein was concomitant with an increase in phospho-Ser15 and acetyl-K382 (Fig. 5B). TP53 is phosphorylated at Ser15 and Ser20 in response to DNA damage, which reduces MDM2 binding and proteasomal degradation of p53 (20). Furthermore, p53 is acetylated in response to cellular stress, and this modification can further stabilize TP53 protein levels and modulate binding activity (21). Activation of TP53 can trigger apoptosis through upregulation of proapoptotic factors such as BBC3 (PUMA), PMAIP1 (NOXA), and BAX (22). The RNA-seq dataset showed a 3.95-fold increase in BBC3 and 1.38-fold increase in PMAIP1 in APTO-253–treated MV4-11 cells. Involvement of DNA damage and cell stress pathways was further interrogated in MV4-11 cells at early time points after treatment with 500 nmol/L APTO-253. An increase in phos-CHEK1 was detected at 1 hour after APTO-253 addition with a peak at approximately 4 hours, suggesting that DNA damage was an early event (Fig. 5C). Following CHEK1 phosphorylation, there was a robust increase in the DDR marker γH2AX by 6 hours. A concentration-dependent increase in γH2AX was detected in all AML lines tested, thereby adding further credence to the concept that APTO-253 triggers the DDR pathway (Fig. 5D). In addition, there was an increase in both MAPK14 phos-T180 and MAPK8 phos-Thr183/pTyr185 at 4- to 6-hour treatment, which indicated signaling through the DDR or ER stress pathways (Fig. 5C). Overall, the data suggest that DNA damage induced by APTO-253 is an early event in the mechanism of APTO-253.

Intracellular pharmacokinetics of APTO-253

Measurement of the kinetics of uptake and efflux of APTO-253 in KG-1 AML cells determined by mass spectrometry indicated a gradual approach to steady state and a rapid initial efflux, but a very prolonged terminal efflux (Supplementary Fig. S6A and S6B). When KG-1 cells were exposed to APTO-253 for either 1 or 6 hours and then placed in drug-free media, the efflux pattern consisted of a rapid phase occurring during the first 30 minutes followed by a prolonged terminal phase, such that significant amounts of APTO-253 were retained in KG-1 cells for longer than 24 hours. Consistent with these data, cellular pharmacokinetic studies disclosed that APTO-253 is transformed intracellularly to a complex containing 1 atom of Fe and 3 molecules of 253 [$Fe(253)_3$] (Supplementary Fig. S6C and S6D; ref. 6). Indeed, the precomplexed $Fe(253)_3$ drug is as potent as the parental APTO-253 monomer in cytotoxicity assays (Fig. 6A). Furthermore, Fe $(253)_3$ complex triggered apoptotic and DNA damage pathways, as measured by c-PARP and γH2AX respectively, in MV-4-11 cells. $Fe(253)_3$ also induced KLF4 and CDKN1A expression and inhibited MYC in a dose-dependent manner (Fig. 6B). However, higher

Published OnlineFirst April 6, 2018; DOI: 10.1158/1535-7163.MCT-17-1209

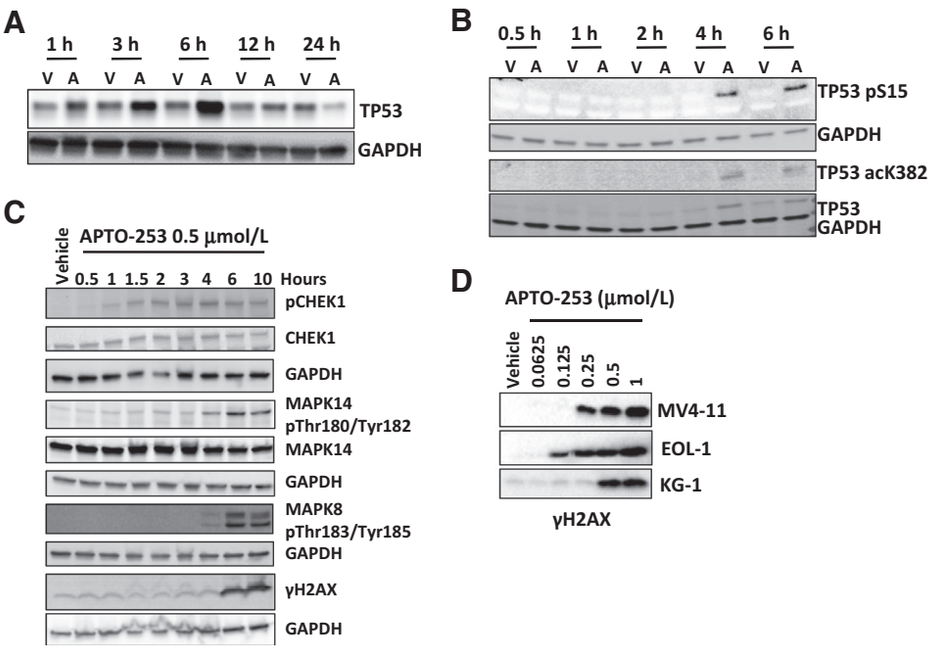

Figure 5.

APTO-253 induces DDR pathways. **A,** Total TP53 protein levels in MV4-11 cells treated with (V) vehicle or 500 nmol/L (A) APTO-253 for increasing periods of time. **B,** Posttranslational modifications of TP53 detected by Western blot analysis in MV4-11 cells treated as in **A**. **C,** Western blot analysis of MV4-11 cells exposed to 500 nmol/L APTO-253. **D,** Western blot analysis of γ-H2AX (H2AX phos-S139) levels in MV4-11, KG-1, and EOL-1 cells treated with APTO-253 for 24 hours at the concentrations noted.

concentrations of $Fe(253)_3$ were required to elicit an equal response to parental APTO-253 in the 24-hour assays (in comparison with 5-day treatment in cytotoxicity assays) likely due to a slower observed influx rate for precomplexed $Fe(253)_3$ (Supplementary Fig. S6E).

APTO-253 stabilizes G-quadruplex sequences

The parental APTO-253 and its intracellular $Fe(253)_3$ form contain certain features, such as metal-coordinating phenanthroline rings and planar structures, that may allow the agent to function as a G-quadruplex (G4) DNA ligand (23, 24). G4 is a dynamic secondary DNA structure caused by guanine-rich regions folding to form planar guanine tetrads, which stack on top of one another (25). G4-specific sequences are found at telomeres and in the promoters of many important oncogenes (26). G4 sequences serve as regulators of gene expression and small-molecule ligands that stabilize G4 quadruplexes have been exploited to downregulate important oncogenes, such as *KIT* and *MYC* (27, 28). Stabilization of G4 motifs in telomere DNA can cause inhibition of telomerase, telomere instability, and deprotection, all of which can trigger DDR pathways (29). Furthermore, origin of DNA replication sites overlap with DNA G4 sequences, and stabilization of G-quadruplex structures at such sites causes stalling of replication forks and cell-cycle arrest (30).

We evaluated the ability of APTO-253 (parental monomeric form of the drug) and $Fe(253)_3$ to bind and stabilize G4 sequences using a modified FRET assay (Supplementary Figs. S7 and S8). TMPyP4, a well-known G4 ligand, and CX-5461, a clinical stage molecule recently reported to have G4-binding properties, were utilized as controls to assess the specificity of APTO-253 and $Fe(253)_3$ for G4-stabilizing activity (25, 31). As expected, CX-5461 was a potent stabilizer of all G4 sequences tested, and TMPyP4 stabilized all G4 motifs except the G4 of the *KIT* gene promoter (Fig. 6C). Interestingly, increasing concentrations of $Fe(253)_3$ stabilized the G4 structures corresponding to the *MYC* and *KIT* gene promoters, rRNA, and telomeres with a similar potency to TMPyP4 (Fig. 6C; Supplementary Fig. S8). Parental monomeric APTO-253 also showed time-dependent stabilization of G4 motifs, but it demonstrated the greatest propensity for stabilizing the *MYC* G4 sequences (Fig. 6C).

To assess selectivity for G4 structures over nonspecific interactions with ds-DNA, the FRET assay was repeated with a self-complimentary oligo that forms a ds-DNA hairpin in solution. Notably, $Fe(253)_3$ demonstrated a much higher degree of selectivity for G4 structures over ds-DNA than did both CX-5461 and TMPyP4, highlighting the fact that APTO-253 is a more discriminating G4 ligand (Fig. 6C; Supplementary Fig. S7B). Gene expression analyses showed that the expression of *MYC* and *KIT* was decreased in AML cells in response to APTO-253 treatment (RNA-seq data, MV4-11 cells 6-hour treatment), but levels of 45s rRNA were not. The lack of effect on 45s rRNA may reflect differences in availability of APTO-253 and/or Fe(253)3 into the rRNA-rich nucleolar region of the nucleus. Nevertheless, APTO-253 clearly can stabilize G4 structures, which provides an explanation for the inhibition of the expression of *MYC* and other genes. We hypothesize that stabilization of G4 motifs by APTO-253 results in single- and double-strand breaks at replication forks and telomeres; this G4-binding capacity of APTO-253 identifies a mechanism by which the drug triggers DDR pathways, cell-cycle arrest, and apoptosis.

Discussion

APTO-253 is currently in clinical development for the treatment of AML because of its efficacy in nonclinical models and the fact that it did not produce myelosuppression in animals or in its initial phase I trial in solid tumor patients (1, 4). The data reported here provide new insights into the mechanism of action of this novel agent that point the way to more precise clinical application and biomarker development. These studies confirmed that APTO-253 is a potent inducer of G_0–G_1 cell-cycle arrest and apoptosis in AML cells. Additional new findings include that APTO-253

Published OnlineFirst April 6, 2018; DOI: 10.1158/1535-7163.MCT-17-1209

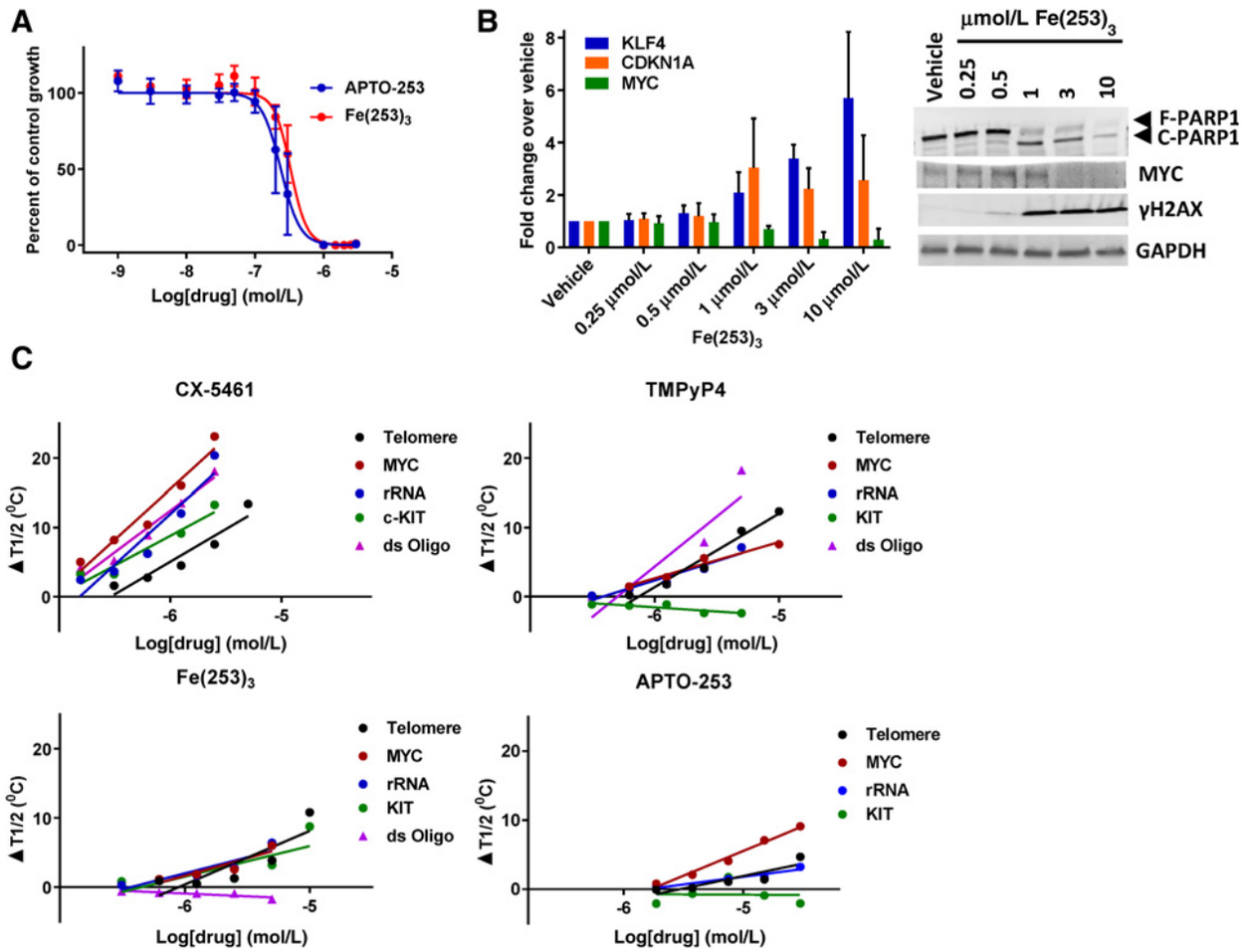

Figure 6.

In vitro and cellular activity of $Fe(253)_3$ complex. **A,** Concentration-response curves for AML cell lines treated for 5 days with parental APTO-253 or $Fe(253)_3$. Cell growth expressed as percent of growth of vehicle-treated cells. Error bars, mean ± SD from 3–5 replicate assays. **B,** Left, KLF4, CDKN1A, and MYC mRNA expression after 24-hour treatment with $Fe(253)_3$ at concentrations listed. Error bars, mean ± SD. Right, Western blot analysis of c-PARP1, MYC, and γH2AX protein levels in MV4-11 cells after 24-hour exposure to vehicle (v) or increasing concentrations of $Fe(253)_3$. **C,** $\Delta T_{1/2}$ values calculated from FRET curves representative examples shown in Supplementary Figs. S7 and S8, with at least three replicates for each curve. The $\Delta T_{1/2}$ of each oligo is plotted against log[drug] mol/L for each compound tested.

produces time- and concentration-dependent downregulation of MYC through effects on both its promoters and mRNA stability, that in many AML cell lines it induces the master transcription factor and tumor suppressor KLF4, and that it induces DNA damage. In addition, the precomplexed iron form of APTO-253, $Fe(253)_3$, causes comparable cytotoxic cellular effects, including apoptosis, DNA damage, and downregulation of MYC expression.

The discovery that ATPO-253, whether in its parental monomeric form or the $Fe(253)_3$ iron complex form, stabilizes G4 motifs in DNA provides an explanation for many of the pharmacodynamic effects of this drug. Stabilization of G4s is known to disrupt telomere stability and stall replication forks, resulting in single- and double-strand DNA breaks (29, 30). Such stabilization of G4 in the *MYC* promoter is thought to function as a gene silencer. This, coupled with targeting of *KIT* and telomere G4 structures by APTO-253, provides a mechanism through which APTO-253 activates DDR pathways that coordinate cell-cycle arrest and promote apoptosis in AML cells. In addition, cells harboring BRCA1/2 mutations are hypersensitive to APTO-253, further supporting a role for DNA damage in APTO-253 mechanism of action. APTO-253 consistently produced upregulation of CDKN1A, which mediates arrest in G_0–G_1 (13). In addition, CDKN1A can be induced after DNA double-strand breaks to block cell-cycle progression to allow for sufficient time to repair DNA (32). In combination with CDKN1A induction, APTO-253 increased *KLF4* gene expression in many AML cell lines, which is known to regulate CDKN1A as part of the G_1 cell-cycle checkpoint (33). KLF4 is also known to be upregulated in response to DNA damage and plays a role in both G_0–G_1 arrest and apoptosis (34, 35). The role of KLF4 in APTO-253 mechanism of action is of interest for future studies. Although the structure of APTO-253 suggests that it might be able to generate reactive oxygen species, no such species have been detected using either molecular sensors or changes in GSH in MV4-11, EOL1, or KG-1 cells.

Published OnlineFirst April 6, 2018; DOI: 10.1158/1535-7163.MCT-17-1209

Activation of CHEK1/2, stabilization of TP53, and induction of E2F1 also indicate that the early events after APTO-253 treatment function to signal for cell-cycle arrest and DNA repair (21–23, 25). Cell-cycle arrest was detected by 2 hours after APTO-253 treatment, whereas upregulation of several proapoptotic factors at both the RNA and protein levels was observed by 6 hours. In addition to activating DNA repair processes, pCHEK1/2 and TP53 can also play a role in triggering apoptosis. If DNA repair fails, p53 can activate apoptosis via upregulation of BAX, BAD, BBC3, or PMAIP1 (22). Increased expression of these proapoptotic factors was detected by RNA-seq analysis of APTO-253–treated MV4-11 cells. It is known that caspase-dependent cleavage of PARP1 is required for apoptosis to proceed. APTO-253 produced robust and early PARP1 cleavage, adding further credence to the hypothesis that APTO-253 functions by triggering DDR pathways. This suggests a level of DNA damage that is catastrophic to the cell and an alteration of transcriptional programs that skew the cell toward apoptosis.

MYC dysregulation is a common oncogenic driver in multiple malignancies, which makes it an attractive potential therapeutic target. However, targeting MYC is challenging due to the complexity of MYC regulation and signaling. Recently, repression of MYC expression by BET bromodomain inhibitors has proven effective at triggering apoptosis in leukemia cells (18). However, bromodomain proteins are present on all active genes, and inhibition of bromodomain proteins can cause severe toxicities and myelosuppression. APTO-253 produced a decrease in MYC expression at both the RNA and protein levels in all AML cell lines tested, and downregulation of MYC paralleled its cytotoxic potency in different AML cells. We detected higher MYC levels in AML lines than in PBMCs from healthy donors, which may be linked to the differential effect of APTO-253 on these types of cells. Recent work demonstrated that coordinated upregulation of TP53 and downregulation of MYC led to efficient clearing of leukemic stem cell populations in CML (36). APTO-253 treatment of MV4-11 produced this same effect, which provides an additional rationale for its development. It has been reported that higher MYC expression correlates with a poor clinical outcome in epithelial ovarian cancer and neuroblastoma, suggesting that APTO-253 may have a beneficial effect against these malignancies (37). Collectively, our data demonstrate a multifaceted mechanism of action for APTO-253, primarily through engagement of G-quadruplex structures, that is uniquely suited to targeting hematopoietic malignancies. Moreover, APTO-253 represents a first-in-class MYC inhibitor that does not cause myelosuppression, making it particularly appropriate for the management of AML patients with compromised bone marrow function.

Disclosure of Potential Conflicts of Interest

H. Zhang is the director of research at Aptose Biosciences, Inc. S.B. Howell reports receiving a commercial research grant as a research contract and is a scientific advisory board member. W.G. Rice is the chairman, president, chief executive officer, and chief scientific officer at Aptose Biosciences. No potential conflicts of interest were disclosed by the other authors.

Authors' Contributions

Conception and design: A. Local, H. Zhang, S.B. Howell, W.G. Rice
Development of methodology: A. Local, H. Zhang
Acquisition of data (provided animals, acquired and managed patients, provided facilities, etc.): A. Local, K.D. Benbatoul, P. Folger, X. Sheng, W.G. Rice
Analysis and interpretation of data (e.g., statistical analysis, biostatistics, computational analysis): A. Local, H. Zhang, K.D. Benbatoul, P. Folger, X. Sheng, S.B. Howell, W.G. Rice
Writing, review, and/or revision of the manuscript: A. Local, H. Zhang, S.B. Howell, W.G. Rice
Administrative, technical, or material support (i.e., reporting or organizing data, constructing databases): A. Local, C.-Y. Tsai
Study supervision: H. Zhang, W.G. Rice

Acknowledgments

We thank Dr. Beth Wilmot and Daniel Bottomly in the laboratory of Dr. Shannon McWeeny at OHSU for QC and mapping of the RNA-seq data, and for generation of gene expression lists and differential expression values.

The costs of publication of this article were defrayed in part by the payment of page charges. This article must therefore be hereby marked *advertisement* in accordance with 18 U.S.C. Section 1734 solely to indicate this fact.

Received December 4, 2017; revised February 21, 2018; accepted April 3, 2018; published first April 6, 2018.

References

1. Huesca M, Lock LS, Khine AA, Viau S, Peralta R, Cukier IH, et al. A novel small molecule with potent anticancer activity inhibits cell growth by modulating intracellular labile zinc homeostasis. Mol Cancer Ther 2009; 8:2586–96.
2. Cukier H, Peralta R, Jin H, Cheng Y, Nedunuri V, Salehi S, et al. Utilization of KLF-4 as a pharmacodynamic biomarker for *in vivo* anticancer activity of a novel small molecule drug LOR-253 [abstract]. In: Proceedings of the 104th Annual Meeting of the American Association for Cancer Research; 2013 Apr 6–10; Washington, DC. Philadelphia (PA): AACR; 2013. Abstract nr 4649.
3. Rice WG, Vellanki A, Lee Y, Lightfoot J, Peralta R, Jamerlan M, et al. APTO-253 induces KLF4 to promote potent *in vitro* pro-apoptotic activity in hematologic cancer cell lines and antitumor efficacy as a single agent and in combination with azacitidine in animal models of acute myelogenous leukemia (AML). Blood 2014; 124:4813.
4. Cercek A, Wheler J, Murray PE, Zhou S, Saltz L. Phase 1 study of APTO-253 HCl, an inducer of KLF4, in patients with advanced or metastatic solid tumors. Invest New Drugs 2015;33:1086–92.
5. Kurtz SE, Bottomly D, Wilmont B, McWeeney SK, Rice WG, Howell SB, et al. Broad activity of APTO-253 in AML and other hematologic malignancies correlates with KFL4 expression level [abstract]. Blood 2015;126:1358.
6. Tsai CY, Sun S, Zhang H, Local A, Su Y, Gross LA, et al. APTO-253 is a new addition to the repertoire of drugs that can exploit DNA BRCA1/2 deficiency. Mol Cancer Ther 2018;17:1167–76.
7. Drygin D, Lin A, Bliesath J, Ho CB, O'Brien SE, Proffitt C, et al. Targeting RNA polymerase I with an oral small molecule CX-5461 inhibits ribosomal RNA synthesis and solid tumor growth. Cancer Res 2011; 71:1418–30.
8. Liao Y, Smyth GK, Shi W. The Subread aligner: fast, accurate and scalable read mapping by seed-and-vote. Nucleic Acids Res 2013;41:e108.
9. De Cian A, Guittat L, Kaiser M, Sacca B, Amrane S, Bourdoncle A, et al. Fluorescence-based melting assays for studying quadruplex ligands. Methods 2007;42:183–95.
10. De Rache A, Mergny JL. Assessment of selectivity of G-quadruplex ligands via an optimised FRET melting assay. Biochimie 2015;115: 194–202.
11. Lum R, Javadi M, Cheng T, Peralta R, Cukier H, Lightfoot J, et al. Induction of KLF4 by LOR-253 as an innovative therapeutic approach to induce apoptosis in acute myeloid leukemia. [abstract]. In: Proceedings of the 105th Annual Meeting of the American Association for Cancer

Published OnlineFirst April 6, 2018; DOI: 10.1158/1535-7163.MCT-17-1209

Research; 2014 Apr 5–9; San Diego, CA. Philadelphia (PA): AACR; 2014. Abstract nr 4544.
12. Wang B, Shen A, Ouyang X, Zhao G, Du Z, Huo W, et al. KLF4 expression enhances the efficacy of chemotherapy drugs in ovarian cancer cells. Biochem Biophys Res Commun 2017;484:486–92.
13. Abbas T, Dutta A. p21 in cancer: intricate networks and multiple activities. Nat Rev Cancer 2009;9:400–14.
14. Dicks N, Gutierrez K, Michalak M, Bordignon V, Agellon LB. Endoplasmic reticulum stress, genome damage, and cancer. Front Oncol 2015; 5:11.
15. Iurlaro R, Munoz-Pinedo C. Cell death induced by endoplasmic reticulum stress. FEBS J 2016;283:2640–52.
16. Tansey WP. Mammalian MYC proteins and cancer. N J Sci 2014; 2014:27.
17. Brondfield S, Umesh S, Corella A, Zuber J, Rappaport AR, Gaillard C, et al. Direct and indirect targeting of MYC to treat acute myeloid leukemia. Cancer Chemother Pharmacol 2015;76:35–46.
18. Mertz JA, Conery AR, Bryant BM, Sandy P, Balasubramanian S, Mele DA, et al. Targeting MYC dependence in cancer by inhibiting BET bromodomains. Proc Natl Acad Sci U S A 2011;108:16669–74.
19. Liu J, Levens D. Making myc. Curr Top Microbiol Immunol 2006; 302:1–32.
20. Lakin ND, Jackson SP. Regulation of p53 in response to DNA damage. Oncogene 1999;18:7644–55.
21. Bode AM, Dong Z. Post-translational modification of p53 in tumorigenesis. Nat Rev Cancer 2004;4:793–805.
22. Roos WP, Kaina B. DNA damage-induced cell death: from specific DNA lesions to the DNA damage response and apoptosis. Cancer Lett 2013;332:237–48.
23. Castor KJ, Mancini J, Fakhoury J, Weill N, Kieltyka R, Englebienne P, et al. Platinum(II) phenanthroimidazoles for targeting telomeric G-quadruplexes. ChemMedChem 2012;7:85–94.
24. Huang HL, Li ZZ, Liang ZH, Yao JH, Liu YJ. Synthesis, cellular uptake, apoptosis, cytotoxicity, cell cycle arrest, interaction with DNA and antioxidant activity of ruthenium(II) complexes. Eur J Med Chem 2011;46:3282–90.
25. Balasubramanian S, Hurley LH, Neidle S. Targeting G-quadruplexes in gene promoters: a novel anticancer strategy? Nat Rev Drug Discov 2011;10:261–75.
26. Hansel-Hertsch R, Di Antonio M, Balasubramanian S. DNA G-quadruplexes in the human genome: detection, functions and therapeutic potential. Nat Rev Mol Cell Biol 2017;18:279–84.
27. Chen BJ, Wu YL, Tanaka Y, Zhang W. Small molecules targeting c-Myc oncogene: promising anti-cancer therapeutics. Int J Biol Sci 2014;10: 1084–96.
28. Rhodes D, Lipps HJ. G-quadruplexes and their regulatory roles in biology. Nucleic Acids Res 2015;43:8627–37.
29. Neidle S. Human telomeric G-quadruplex: the current status of telomeric G-quadruplexes as therapeutic targets in human cancer. FEBS J 2010;277: 1118–25.
30. Besnard E, Babled A, Lapasset L, Milhavet O, Parrinello H, Dantec C, et al. Unraveling cell type-specific and reprogrammable human replication origin signatures associated with G-quadruplex consensus motifs. Nat Struct Mol Biol 2012;19:837–44.
31. Xu H, Di Antonio M, McKinney S, Mathew V, Ho B, O'Neil NJ, et al. CX-5461 is a DNA G-quadruplex stabilizer with selective lethality in BRCA1/2 deficient tumours. Nat Commun 2017;8:14432.
32. Nowsheen S, Yang ES. The intersection between DNA damage response and cell death pathways. Exp Oncol 2012;34:243–54.
33. Tetreault MP, Yang Y, Katz JP. Kruppel-like factors in cancer. Nat Rev Cancer 2013;13:701–13.
34. Ghaleb AM, Yang VW. Kruppel-like factor 4 (KLF4): What we currently know. Gene 2017;611:27–37.
35. Guan H, Xie L, Leithauser F, Flossbach L, Moller P, Wirth T, et al. KLF4 is a tumor suppressor in B-cell non-Hodgkin lymphoma and in classic Hodgkin lymphoma. Blood 2010;116:1469–78.
36. Abraham SA, Hopcroft LE, Carrick E, Drotar ME, Dunn K, Williamson AJ, et al. Dual targeting of p53 and c-MYC selectively eliminates leukaemic stem cells. Nature 2016;534:341–6.
37. Jung M, Russell AJ, Liu B, George J, Liu PY, Liu T, et al. A Myc Activity signature predicts poor clinical outcomes in myc-associated cancers. Cancer Res 2017;77:971–81.

Published OnlineFirst April 6, 2018; DOI: 10.1158/1535-7163.MCT-17-1209

Molecular Cancer Therapeutics

APTO-253 Stabilizes G-quadruplex DNA, Inhibits MYC Expression, and Induces DNA Damage in Acute Myeloid Leukemia Cells

Andrea Local, Hongying Zhang, Khalid D. Benbatoul, et al.

Mol Cancer Ther 2018;17:1177-1186. Published OnlineFirst April 6, 2018.